

# Identifying Long Radio Transients with Accompanying X-Ray Emission as Disk-Jet Precessing Black Holes: The Case of ASKAP J1832-0911

Antonios Nathanail\*

Research Center for Astronomy and Applied Mathematics, Academy of Athens, Athens 11527, Greece

Received June 18, 2025; Accepted — 2025

## ABSTRACT

**Aims.** In this work we investigate whether the 2 min bursts every 44 min from ASKAP J1832-0911 can be explained by Lense-Thirring precession of an intermediate-mass black hole (IMBH) accretion disk launching a Blandford-Znajek jet, as an alternative to magnetar or white-dwarf models.

**Methods.** We derive the Lense-Thirring period  $P_{\text{LT}} = \frac{\pi G M}{a c^3} r^3$  and solve  $P_{\text{LT}} = 44$  min for black-hole mass  $M$  and dimensionless radius  $r = R/R_g$ . We estimate the equipartition field  $B$  at  $r$ , compute the Blandford-Znajek power  $P_{\text{BZ}}$ , and the power expected from a gap at the black hole magnetosphere, and compare the resulting jet luminosity to the observed radio and X-ray fluxes at  $D \approx 4.5$  kpc. We also evaluate expected high-frequency variability and the angular size for Very Long Baseline Interferometry (VLBI) observations.

**Results.** For  $a \sim 0.3-0.9$ , an IMBH with  $M \sim 10^3-10^5 M_\odot$  yields  $r \sim 10-40 R_g$  and  $P_{\text{LT}} = 44$  min. Equipartition gives  $B \sim 10^5$  G at  $r$ , leading to  $P_{\text{BZ}} \sim 10^{35-39}$  erg s $^{-1}$ . With radiative efficiency  $\epsilon_j \sim 10^{-2}-10^{-1}$ , the predicted  $L_{\text{jet}} \sim 10^{34-36}$  erg s $^{-1}$  matches the observed  $F_X \sim 10^{-12}$  erg cm $^{-2}$  s $^{-1}$  and radio flux, variability on  $\lesssim 100$  s could be a smoking gun of this model.

**Conclusions.** The IMBH precessing-jet model simultaneously explains the periodicity, energetics, and duty cycle of ASKAP J1832-0911. Only high-time-resolution X-ray timing (to exclude  $\sim$ s pulsations) and multi-frequency radio polarimetry (to confirm a flat, low-polarization spectrum) can definitively distinguish it from magnetar or white-dwarf scenarios.

**Key words.** black hole physics – resistivity – accretion – accretion discs – magnetic reconnection – magneto-hydrodynamics

## 1. Introduction

Long radio transients -sources whose emission appears abruptly and fades over timescales ranging from minutes to days-have long challenged our understanding of compact-object astrophysics (Hurley-Walker et al. 2022, 2023). A handful of Galactic Center Radio Transients (GCRTs), such as GCRT J1745-3009 with its 10 min bursts every 77 min, exemplify periodic behavior on timescales of tens of minutes (Hyman et al. 2005). More recently, ASKAP J1832-0911 was discovered as a bright radio-and X-ray transient located in the Scutum spiral arm at an estimated distance of 4.5 kpc. ASKAP observations reveal 2 min-long radio flares (at GHz frequencies, with peak flux densities of order 10 mJy) recurring every 44 min, and simultaneous X-ray observations detect 2 min X-ray pulses (with fluxes  $10^{-12}$  erg cm $^{-2}$  s $^{-1}$  in 0.5-10 keV) at the same 44 min cadence (Wang et al. 2025). Such a precise, multiwavelength periodicity over tens of minutes is exceedingly rare among known transients.

Two leading compact-object interpretations are followed: a highly magnetized neutron star (magnetar) whose beamed emission sweeps past Earth for 2 min each 44 min rotation (Cooper & Wadiasingh 2024), and an ultracompact white-dwarf (WD) binary in which magnetic gating produces synchronized radio and X-ray bursts every orbital period. A slowly rotating magnetar with occasional "heartbeat" flares can reproduce similar with the observed X-ray energetics Pons & Viganò (2019), while analogous hour-period WD-WD binaries as possible progenitors of

long radio flares (Qu & Zhang 2025) with X-rays (Schwope et al. 2023), or a WD with a pulsar (Katz 2022). Although these models capture some aspects of the 44 min duty cycle, each faces challenges-e.g., maintaining a 44 min spin despite rapid magnetar spin-down, or explaining coherent X-ray emission from a WD shock engine over minute-long intervals.

Here, we propose instead that ASKAP J1832-0911 is powered by an intermediate-mass black hole (IMBH,  $M 10^3 - 10^5 M_\odot$ ) with a tilted accretion disk whose inner regions rigidly precess via the Lense-Thirring effect. In this picture, a relativistic jet, launched by Blandford-Znajek extraction of spin energy, sweeps across our line of sight for 2 min every 44 min, producing the observed radio and X-ray flares. IMBHs have been invoked to explain ultraluminous X-ray sources (ULXs; e.g., Farrell et al. (2009)), dynamical signatures in globular clusters (e.g., Gebhardt et al. (2005)), and low-luminosity AGN in dwarf galaxies (Mezcua 2017). Formation channels include direct collapse of Population III stars, runaway mergers in dense star clusters (Portegies Zwart & McMillan 2002), and the cores of dwarf galaxies (Reines & Volonteri 2015). If an IMBH of  $M 10^5 M_\odot$  resides in a Galactic plane cluster or an unrecognized dwarf satellite, its inner disk could naturally precess on a 44 min timescale at radii  $r \sim 30 R_g$ , while accumulating sufficient magnetic flux to power the observed jet luminosity.

This Letter is organized as follows. In Section 2, we outline a simple geometric model for Lense-Thirring precession of a tilted ring or disk, derive the relationship between black-hole mass  $M$ , disk radius  $r (= R/R_g)$ , and precession period, and show how the 44 min cycle constrains  $M$  and  $r$ . In Section 3, we ap-

\* anathanail@academyofathens.gr

ply the model to derive viable IMBH mass ranges and disk radii, estimate the equipartition magnetic field at  $r$  and the corresponding Blandford-Znajek jet power, and compare these predictions to the observed radio and X-ray luminosities. We also discuss known AGN jet precession as a sanity check on our IMBH scaling (e.g. M87's 11 yr cycle). In Section 4, we contrast the IMBH scenario with magnetar and white-dwarf alternatives by summarizing key observational discriminants (e.g., X-ray spectral components, spin pulsations, radio polarization) and show why a stellar-mass XRB with subhour precession is effectively ruled out by analogues such as SS 433, Her X-1, and LMC X-4. We conclude with suggestions for targeted follow-up observations to definitively distinguish among these models.

## 2. Lense-Thirring Precession and Visibility Geometry

To assess whether a tilted, rigidly precessing disk (and its jet) can naturally produce 2 min-long flares every 44 min, we first derive the Lense-Thirring (LT) precession period for a test ring at radius  $R$  around a spinning black hole. We then construct a simple geometric model (Maccarone 2002; Liska et al. 2018; Liska et al. 2019) and relate the jet's half-opening angle and disk tilt to the observed duty cycle.

### 2.1. Lense-Thirring Precession Period

A Kerr black hole of mass  $M$  and dimensionless spin  $a$  has angular momentum  $J = a \frac{GM^2}{c}$ . A test particle (or narrow ring) at Boyer-Lindquist radius  $R$  experiences a nodal precession frequency  $\Omega_{LT}(R)$  given by (Wilkins 1972; Stella & Vietri 1998; Fragile et al. 2007):

$$\Omega_{LT}(R) = \frac{2 G J}{c^2 R^3} = \frac{2 a G^2 M^2}{c^3 R^3}. \quad (1)$$

Hence the LT precession period is

$$P_{LT}(R) = \frac{2\pi}{\Omega_{LT}(R)} = \frac{2\pi}{\frac{2 a G^2 M^2}{c^3 R^3}} = \frac{\pi c^3 R^3}{a G^2 M^2}. \quad (2)$$

Measuring distance in gravitational-radius units,

$$R_g = \frac{GM}{c^2}, \quad r \equiv \frac{R}{R_g}, \quad (3)$$

and substituting  $R = r R_g$  into Eq. (2) gives

$$P_{LT}(r) = \frac{\pi G M}{a c^3} r^3 = (1.55 \times 10^{-5}) \frac{m}{a} r^3 \quad [\text{s}], \quad (4)$$

where  $M = m M_\odot$  and  $G M_\odot/c^3 \approx 4.9 \times 10^{-6}$  s. Requiring  $P_{LT} = 44$  min = 2640 s yields the constraint

$$m r^3 = 1.703 \times 10^8 a. \quad (5)$$

### 2.2. Visibility Geometry and Duty Cycle

If the inner disk at radius  $r$  is tilted by angle  $\psi$  relative to the black-hole spin axis, it precesses at  $\Omega_{LT}$ . Assuming the jet is launched along the disk normal (Maccarone 2002; Fragile et al. 2007; Liska et al. 2018), and that our line of sight is inclined by

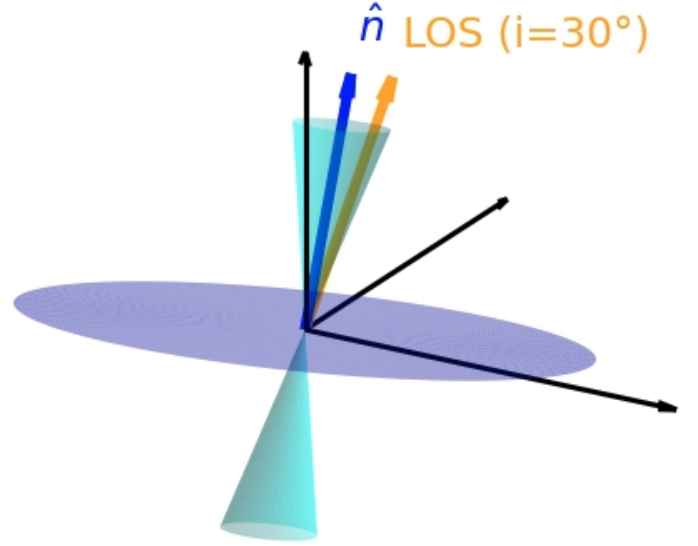


**Fig. 1.** Geometry of the precessing disk-jet system. The blue disk is tilted by  $\psi$  relative to the black hole spin axis (vertical), and the cyan cones show the jet with half-opening angle  $\alpha$ . As the system precesses, the disk normal (blue arrow) periodically aligns with the observer's line of sight (orange arrow) and the jet beam crosses the LOS, producing the observed 2 min flares every 44 min. An accompanying animation is available here.

$i$  to the spin axis, the instantaneous angle  $\theta(t)$ <sup>1</sup> between jet axis and observer satisfies (Caproni et al. 2006; Maccarone 2002)

$$\cos \theta(t) = \cos \psi \cos i + \sin \psi \sin i \cos(\Omega_{LT} t). \quad (6)$$

For a jet with half-opening angle  $\alpha$ , it is visible whenever  $\theta(t) \leq \alpha$ . Defining  $\Delta t$  as the total "on" time per cycle  $P_{LT}$ , one finds at the entry/exit points  $\theta = \alpha$ :

$$\cos \alpha = \cos \psi \cos i + \sin \psi \sin i \cos\left(\pi \frac{\Delta t}{P_{LT}}\right). \quad (7)$$

Setting  $\Delta t = 2$  min and  $P_{LT} = 44$  min (so  $\pi \Delta t / P_{LT} = \pi/22$ ) shows that even modest tilts  $\psi \sim 10^\circ - 30^\circ$  and inclinations  $i \sim 30^\circ - 70^\circ$  yield small  $\alpha \sim 5^\circ - 15^\circ$ , reproducing the 2 min/44 min duty cycle (cf. Maccarone 2002; Liska et al. 2019).

In Fig. 1 we present a schematic of the tilted accretion disk, its precessing jet cone, and the viewing geometry. An animation illustrating a disk tilt of  $\psi = 20.6^\circ$ , jet half-opening angle  $\alpha = 10^\circ$ , and observer inclination  $i = 30^\circ$ , showing how the cone sweeps across our line of sight every 44 min, is available here.

## 3. IMBH Mass Constraints, Jet Power, and Variability

Using the Lense-Thirring precession relation (Eq. 5), we show that an IMBH ( $M \sim 10^3 - 10^5 M_\odot$ ) naturally reproduces  $P_{LT} = 44$  min at radii  $r \sim 5 - 30$ . We then estimate the magnetic field strength at  $r$ , compute the Blandford-Znajek jet power, compare it to the observed radio/X-ray luminosities (for  $D \simeq 4.5$  kpc), and discuss small-scale variability and VLBI-scale imaging.

<sup>1</sup> Using the relation of this angle from the dot product of the line of sight and the disk normal unit vectors and allowing the disk normal to precess by an azimuthal angle  $\phi = \Omega_{LT} t$ , we arrive at Eq. 6.

### 3.1. Mass-Radius Solutions for $P_{\text{LT}} = 44$ min

We need a precession with a period of 44 min, so we plug  $P_{\text{LT}} = 2640$  s into Eq. (4) and assume  $a \sim 0.3\text{--}0.9$ , which yields  $r = \left(\frac{1.703 \times 10^8 a}{m}\right)^{1/3}$ . and to check where the rigid precession ring is we find:

- $m = 10^3$ ,  $a = 0.5$ :  $r = (8.53 \times 10^4)^{1/3} \approx 44$ .
- $m = 10^4$ ,  $a = 0.5$ :  $r = (8.53 \times 10^3)^{1/3} \approx 20.4$ .
- $m = 10^5$ ,  $a = 0.5$ :  $r = (8.53 \times 10^2)^{1/3} \approx 9.5$ .
- $m = 10^6$ ,  $a = 0.5$ :  $r = (8.53 \times 10^1)^{1/3} \approx 4.4$ .

Thus  $M = 10^3\text{--}10^5 M_\odot$  corresponds to  $r \approx 9\text{--}44 R_g$ , consistent with inner-disk extents. By contrast,  $m \sim 10$  yields  $r \approx 204$ , far outside typical XRB disks (Fragile et al. 2007; Liska et al. 2018), and cannot precess rigidly on 44 min timescales. Therefore, the IMBH regime is the only one that locates a rigidly precessing ring at  $r \sim 4\text{--}40 R_g$ . However, at the small-radius end ( $r \leq 5 R_g$ ), frame-dragging is so strong that the Bardeen-Petterson effect can overcome viscous communication, forcing the innermost flow to realign with the black hole's equatorial plane and potentially breaking the assumption of perfectly rigid precession (Bardeen & Petterson 1975).

### 3.2. Magnetic Field, Power and Emission

Assume near-Eddington accretion for  $M = 10^4 M_\odot$ :

$$L_{\text{Edd}} = 1.3 \times 10^{38} \frac{M}{M_\odot} \text{ erg/s} = 1.3 \times 10^{42} \text{ erg/s},$$

$$\dot{M}_{\text{Edd}} \approx \frac{L_{\text{Edd}}}{0.1 c^2} \sim 1.4 \times 10^{21} \text{ g/s}.$$

At  $r = 20 R_g$ ,  $R = 3.0 \times 10^{10}$  cm,  $v_{\text{ff}} \sim c$ , the density is  $\rho \sim \frac{M_{\text{Edd}}}{4\pi R^2 c} \approx 4.3 \times 10^{-12}$  g/cm<sup>3</sup>, and the ram pressure  $P_{\text{ram}} \sim \rho c^2 \approx 3.87 \times 10^9$  dyn/cm<sup>2</sup>. Equipartition,  $B^2/(8\pi) \approx P_{\text{ram}}$ , gives

$$B \sim \sqrt{8\pi P_{\text{ram}}} \sim 3.1 \times 10^5 \text{ G},$$

so we adopt  $B \sim 10^4\text{--}10^6$  G at  $r \sim 10\text{--}40 R_g$ .

The Blandford-Znajek power is  $P_{\text{BZ}} \sim \frac{1}{32} a^2 B^2 R_g^2 c$  (Blandford & Znajek 1977; Tchekhovskoy et al. 2010). For  $a = 0.5$ ,  $B = 2 \times 10^5$  G, and  $R_g = 1.5 \times 10^9$  cm,  $P_{\text{BZ}} \approx 2.1 \times 10^{37}$  erg/s. Allowing  $B = 10^4\text{--}10^6$  G gives  $P_{\text{BZ}} \sim 10^{35\text{--}39}$  erg/s. A radiative efficiency  $\epsilon_j \sim 10^{-2}\text{--}10^{-1}$  yields

$$L_{\text{jet}} = \epsilon_j P_{\text{BZ}} \sim 10^{33\text{--}38} \text{ erg/s}.$$

In the Appendix A we discuss the possibility of observing the jet through VLBI.

The combination of a compact emission zone (either at the jet base or within a narrow magnetospheric gap) and a low-density plasma environment minimizes Faraday rotation and depolarization, allowing intrinsically coherent radiation to retain a high degree of linear polarization. In such regions, the magnetic field is both strong and ordered on small scales, naturally favoring maser-like or bunching instabilities that can generate bright, narrow-band radio bursts.

In addition to the Blandford-Znajek jet, a narrow vacuum gap in the black hole magnetosphere could also provide a compact, highly ordered emission region capable of producing coherent, highly polarized bursts. In such a gap the available potential drop is  $\Delta_{\text{gap}} \approx \frac{\Omega_{\text{BH}} B r_g^2}{c}$ , where  $\Omega_{\text{BH}} = a c / 2 r_g$  is the angular frequency of the event horizon. The produced electric current through the Goldreich-Julian characteristic charge density

$n_{\text{GJ}} = \Omega_{\text{BH}} B / 2\pi e c$ , is  $I_{\text{GJ}} \approx n_{\text{GJ}} e c \pi r_g^2 \sim \Omega_{\text{BH}} B r_g^2 / 2c$ . So that the gap power  $L_{\text{gap}} \sim \Delta_{\text{gap}} I_{\text{GJ}} \sim 10^{37\text{--}38}$  erg/s for  $M \sim 10^4 M_\odot$ ,  $B \sim 2 \times 10^5$  G, and  $a = 0.5$ . Particle-in-cell simulations of black hole gap discharges show that rapid plasma oscillations can lead to charge bunching and pair cascades (Levinson & Cerutti 2018; Yuan et al. 2025). Thus, whether emerging from the jet-launching region or from a magnetospheric gap, a compact, ordered field geometry can explain the observed coherent, highly polarized radio pulses.

### 3.3. Observed Fluxes and Efficiency Constraints

At an assumed distance  $D = 4.5$  kpc ( $\approx 1.4 \times 10^{22}$  cm) (Wang et al. 2025), a luminosity  $L_{\text{obs}}$  corresponds to flux  $F_{\text{obs}} = \frac{L_{\text{obs}}}{4\pi D^2}$ . ASKAP observations find peak radio flux densities  $S_\nu \sim 10$  mJy at  $\nu \sim 1.3$  GHz. Taking a flat spectrum ( $\alpha \approx 0$ ), the radio luminosity at  $\nu = 1.3$  GHz is

$$\begin{aligned} L_{\text{radio}} &\sim 4\pi D^2 S_\nu \approx 4\pi (1.4 \times 10^{22})^2 \times (10^{-2} \text{ Jy}) \\ &\approx 2.5 \times 10^{29} \text{ erg s}^{-1} \text{ Hz}^{-1} \end{aligned}$$

or  $\nu L_\nu \sim 3 \times 10^{38}$  erg/s when integrated over a broad radio band ( $\Delta\nu \sim 10^9$  Hz). X-ray follow-ups find  $F_X \sim 10^{-12}$  erg cm<sup>-2</sup> s<sup>-1</sup> (0.5–10 keV), so

$$L_X \sim 4\pi D^2 F_X \approx 4\pi (1.4 \times 10^{22})^2 \times 10^{-12} \sim 2.5 \times 10^{34} \text{ erg/s}.$$

Thus the combined radio + X-ray luminosity during each 2 min "on"-pulse is  $\sim 10^{34\text{--}38}$  erg/s. Comparing to  $P_{\text{BZ}} \sim 10^{35\text{--}39}$  erg/s, we see that a modest radiative efficiency  $\epsilon_j \sim 10^{-2}\text{--}10^{-1}$  suffices to power the observed fluxes.

Demanding  $\epsilon_j \gtrsim \frac{L_{\text{obs}}}{P_{\text{BZ}}}$  sets a lower limit on  $B$ . If  $L_X + L_{\text{radio}} \sim 10^{36}$  erg/s in total, and we require  $\epsilon_j \lesssim 0.1$ , then  $P_{\text{BZ}} \gtrsim 10^{37}$  erg/s, implying  $B \gtrsim 10^5$  G at  $r \sim 20 R_g$ . This is fully consistent with our equipartition estimate  $B \sim 10^5$  G. Conversely, if  $B$  were as low as  $10^4$  G,  $P_{\text{BZ}} \sim 10^{35}$  erg/s, and achieving  $L_{\text{obs}} \sim 10^{36}$  erg/s would require  $\epsilon_j > 1$ , which is unphysical. Hence we infer  $B \sim 10^5\text{--}10^6$  G as the most plausible range, consistent with near-Eddington inflow at  $r \sim 10\text{--}30 R_g$ .

Inside the precessing region, the jet-disk system may exhibit additional, rapid variability on the local dynamical or accretion timescale. In geometric units, the light-crossing time of  $1 R_g$  is  $t_g = \frac{G M}{c^3} \approx 4.9 \times 10^{-6}$  s ( $\times (\frac{M}{M_\odot})$ ). For  $M = 10^4 M_\odot$ ,  $t_g \approx 4.9 \times 10^{-2}$  s, which is very small compared with the 44 min precession. Also, short-wavelength fluctuations at the inner jet footpoint would occur on  $\sim 10 t_g$  ( $\sim 0.5$  s) due to rapid accretion in tilted disks (Dexter & Fragile 2013) and/or plasmoid formation seen in numerical simulations of accreting black holes (Nathanail et al. 2020; Ripperda et al. 2020), most probably well below any detectable variability. However, flux eruption events which are a prominent feature of strongly magnetized accretion onto a black hole, occur every  $100\text{--}1000 t_g \approx 5\text{--}50$  s (Liska et al. 2019; Ripperda et al. 2022; Nathanail et al. 2025) and could be responsible for the high variability seen in the X-rays.

## 4. Discussion

In this Letter we investigate the possibility that the 2 min bursts every 44 min from ASKAP J1832-0911 can be explained by an intermediate-mass black hole (IMBH) and a precessing accretion disk launching a Blandford-Znajek jet, as an alternative to magnetar or white-dwarf models. The Lense-Thirring precession

constraint,  $P_{\text{LT}} = \frac{\pi G M}{a c^3} r^3 = 44 \text{ min}$  which for  $a \sim 0.3\text{--}0.9$  yields  $r \sim 10\text{--}40 R_g$  when  $M \sim 10^3\text{--}10^5 M_\odot$ .

IMBH mass-radius solutions of  $M \sim 10^3\text{--}10^5 M_\odot$  correspond to  $r \sim 9\text{--}44 R_g$ , placing the precessing ring well within plausible inner-disk extents. By contrast, a  $\sim 10\text{--}30 M_\odot$  BH would require  $r \sim 443 R_g$ , which cannot precess rigidly on a 44 min timescale.

An estimated Blandford-Znajek jet  $L_{\text{jet}} \sim 10^{33\text{--}38} \text{ erg/s}$ , easily reproduces the observed  $\sim 10^{34\text{--}36} \text{ erg/s}$  in radio + X-rays at  $D \simeq 4.5 \text{ kpc}$ .

Characteristic inner-disk timescales ( $t_g \sim 0.5 \text{ s}$ , MHD flux eruptions  $\sim 50 \text{ s}$ ) can be responsible for the rapid variability in the X-rays in the 2 min integration, and the 44 min precession remains the only coherent clock.

The main observational tests that uniquely identify a precessing-disk IMBH as the engine behind ASKAP J1832-0911, distinguishing it from both magnetar and white-dwarf models are the following (amore extended discussion on this on Appendix B. All known magnetars spin in the 2-12 s range and exhibit large-fraction soft X-ray pulsations, whereas the IMBH jet predicts easily a 2 min / 44 min duty cycle and could potentially accommodate some variability due to either accretion or pair cascades. Similarly, intermediate-polar white dwarfs display spin/orbital periods of  $10^2\text{--}10^5 \text{ s}$  and characteristic hard bremsstrahlung spectra, neither of which are seen in this source. Finally, only an LT-precessing IMBH disk can maintain a stable 2 min / 44 min duty cycle over years without invoking fine-tuned phase locks or state transitions.

**Acknowledgements.** The author was supported by the Hellenic Foundation for Research and Innovation (ELIDEK) under Grant No 23698, and by computational time granted from the National Infrastructures for Research and Technology S.A. (GRNET S.A.) in the National HPC facility - ARIS - under project ID 16033.

**Data Availability.** The data underlying this article will be shared on reasonable request to the corresponding author.

## References

Bardeen, J. M. & Petterson, J. A. 1975, *Astrophys. J.*, 195, L65  
 Belloni, T. E., ed. 2010, *Lecture Notes in Physics*, Berlin Springer Verlag, Vol. 794, The Jet Paradigm  
 Belloni, T. M., Klein-Wolt, M., Méndez, M., van der Klis, M., & van Paradijs, J. 2000, *Astronomy & Astrophysics*, 355, 271  
 Blandford, R. D. & Znajek, R. L. 1977, *Mon. Not. R. Astron. Soc.*, 179, 433  
 Caproni, A., Livio, M., Abraham, Z., & Mosquera Cuesta, H. 2006, *Astrophysical Journal*, 653, 112  
 Clarkson, W. I., Charles, P. A., Coe, M. J., et al. 2003, *Monthly Notices of the Royal Astronomical Society*, 339, 447  
 Cooper, A. J. & Wadiasingh, Z. 2024, *Monthly Notices of the Royal Astronomical Society*, 533, 2133  
 Corbel, S., Nowak, M. A., Fender, R. P., Tzioumis, A. K., & Markoff, S. 2003, *Astronomy & Astrophysics*, 400, 1007  
 Dexter, J. & Fragile, P. C. 2013, *MNRAS*, 432, 2252  
 Duncan, R. C. & Thompson, C. 1992, *Astrophys. J.*, 392, L9  
 Enoto, T., Shibata, S., Kitaguchi, T., et al. 2017, *ApJS*, 231, 8  
 Farrell, S. A., Webb, N. A., Barret, D., Godet, O., & Rodrigues, J. M. 2009, *Nature*, 460, 73  
 Fender, R. P., Belloni, T. M., & Gallo, E. 2004, *Mon. Not. R. Astron. Soc.*, 355, 1105  
 Fragile, P. C., Blaes, O. M., Anninos, P., & Salmonson, J. D. 2007, *ApJ*, 668, 417  
 Gebhardt, K., Rich, R. M., & Ho, L. C. 2005, *The Astrophysical Journal*, 634, 1093  
 Harding, A. K. & Lai, D. 2006, *Reports on Progress in Physics*, 69, 2631  
 Heemskerk, M. H. M. & van Paradijs, J. 1989, *Astronomy & Astrophysics*, 223, 154  
 Hurley-Walker, N., Rea, N., McSweeney, S. J., et al. 2023, *Nature*, 619, 487  
 Hurley-Walker, N., Zhang, X., Bahramian, A., et al. 2022, *Nature*, 601, 526  
 Hyman, S. D., Lazio, T. J. W., Kassim, N. E., et al. 2005, *Nature*, 434, 50

Kaspi, V. M. 2010, *Proceedings of the National Academy of Sciences*, 107, 7147  
 Kaspi, V. M. & Beloborodov, A. M. 2017, *Annual Review of Astronomy and Astrophysics*, 55, 261  
 Katz, J. I. 2022, *Astrophysics and Space Science*, 367  
 Levinson, A. & Cerutti, B. 2018, *A&A*, 616, A184  
 Liska, M., Hesp, C., Tchekhovskoy, A., et al. 2018, *Mon. Not. R. Astron. Soc.*, 474, L81  
 Liska, M., Tchekhovskoy, A., Ingram, A., & van der Klis, M. 2019, *MNRAS*, 487, 550  
 Maccarone, T. 2002, *Monthly Notices of the Royal Astronomical Society*, 336, 1371  
 Makishima, K., Kubota, A., Mizuno, T., et al. 2000, *The Astrophysical Journal*, 535, 632  
 Margon, B. 1984, *Annual Review of Astronomy and Astrophysics*, 22, 507  
 Merloni, A., Heinz, S., & di Matteo, T. 2003, *Monthly Notices of the Royal Astronomical Society*, 345, 1057  
 Mezcuca, M. 2017, *International Journal of Modern Physics D*, 26, 1730021  
 Nathanail, A., Fromm, C. M., Porth, O., et al. 2020, *Mon. Not. R. Astron. Soc.*, 495, 1549  
 Nathanail, A., Mizuno, Y., Contopoulos, I., et al. 2025, *A&A*, 693, A56  
 Patterson, J. 1994, *Publications of the Astronomical Society of the Pacific*, 106, 209  
 Petterson, J. A. 1975, *The Astrophysical Journal*, 201, L61  
 Pons, J. A. & Viganò, D. 2019, *Living Reviews in Computational Astrophysics*, 5, 3  
 Portegies Zwart, S. F. & McMillan, S. L. W. 2002, *The Astrophysical Journal*, 576, 899–907  
 Qu, Y. & Zhang, B. 2025, *ApJ*, 981, 34  
 Reines, A. E. & Volonteri, M. 2015, *The Astrophysical Journal*, 813, 82  
 Ripperda, B., Bacchini, F., & Philippov, A. A. 2020, *Astrophys. J.*, 900, 100  
 Ripperda, B., Liska, M., Chatterjee, K., et al. 2022, *Astrophys. J. Lett.*, 924, L32  
 Schwöpe, A., Marsh, T. R., Standke, A., et al. 2023, *A&A*, 674, L9  
 Stella, L. & Vietri, M. 1998, *Astrophysical Journal Letters*, 492, L59  
 Tchekhovskoy, A., Narayan, R., & McKinney, J. C. 2010, *Astrophys. J.*, 711, 50  
 Turolla, R., Zane, S., & Watts, A. L. 2015, *Reports on Progress in Physics*, 78, 116901  
 Wang, Z., Rea, N., Bao, T., et al. 2025, *Nature*, 619, 487–490  
 Warner, B. 1995, *Cataclysmic Variable Stars* (Cambridge University Press)  
 Wilkins, D. C. 1972, *Phys. Rev. D*, 5, 814  
 Yuan, Y., Chen, A. Y., & Luepker, M. 2025, *ApJ*, 985, 159

## Appendix A: VLBI-Scale Jet Size and Resolvability

A final test is whether the precessing jet can be spatially resolved with Very-Long-Baseline Interferometry (VLBI). If the jet originates near  $r \approx 20 R_g$ , then its transverse radius at launch is of order

$$R_{\text{jet}} \sim \alpha r R_g,$$

where  $\alpha$  is the jet's half-opening angle, say  $\alpha \approx 10^\circ \approx 0.1745$  rad. Thus

$$R_{\text{jet}} \sim 0.1745 \times 20 \times 1.5 \times 10^9 \text{ cm} \approx 5 \times 10^9 \text{ cm}.$$

Assuming the jet remains collimated on larger scales but starts with a cylindrical cross-section of radius  $5 \times 10^9$  cm, its angular size at  $D = 4.5$  kpc is

$$\theta \sim \frac{5 \times 10^9}{4.5 \times 10^{21}} \approx 5.8 \times 10^{-13} \text{ rad} \approx 0.12 \mu\text{as}.$$

Even if the jet expands conically by a factor of 100 before becoming optically thin (i.e. radius  $\sim 2.6 \times 10^{11}$  cm),  $\theta \sim 12 \mu\text{as}$ , still below typical VLBI resolution at 1.3 GHz ( $\sim 200 \mu\text{as}$ ). Only future space-VLBI at higher frequencies could hope to resolve any structure. Therefore, direct imaging of the precessing jet is effectively impossible with current VLBI; the only observable is time-dependent brightness modulation ("hot spot" lighting up as the beam swings by).

## Appendix B: Discriminating IMBH, Magnetar and White-Dwarf Scenarios

In this section, we summarize the "smoking-gun" tests that distinguish a precessing-disk IMBH from alternative magnetar or white-dwarf models, and explain why a stellar-mass ( $\sim 10 - 30 M_\odot$ ) black-hole X-ray binary (XRB) is effectively ruled out short of observing a state transition lasting months-years that temporarily erases and then restores the 2 min / 44 min pattern.

### Appendix B.1: Magnetar Model Versus IMBH Jet

All known magnetars spin with  $P_{\text{spin}} \sim 2 - 12$  s and exhibit coherent pulsations in soft X-rays (0.5-10 keV) with large pulsed fractions ( $\sim 10 - 50\%$ ) (e.g., Pons & Viganò 2019; Kaspi & Beloborodov 2017). A slowly rotating ( $\sim 44$  min) magnetar would spin down catastrophically fast ( $\dot{P} \sim 10^{-9} - 10^{-8}$  s/s for  $B \sim 10^{14} - 10^{15}$  G), making long-term stability impossible (Duncan & Thompson 1992; Harding & Lai 2006). By contrast, an IMBH jet model predicts  $\sim$ s-scale variability; in the 2 min precession on window and, at most, high-frequency flickering on  $\lesssim 10^2$  s timescales (Liska et al. 2018). Deep, high-time-resolution X-ray timing can rule out any  $P_{\text{spin}} < 12$  s.

Persistent magnetar spectra are well modeled by one or two blackbodies ( $kT \sim 0.3 - 0.6$  keV) plus a hard power-law tail ( $\Gamma \sim 2 - 4$ ) (Enoto et al. 2017; Turolla et al. 2015), with no cool ( $< 0.1$  keV) disk component. An IMBH, however, should show a multicolor disk blackbody peaking at  $kT_{\text{in}} \sim 0.05 - 0.1$  keV (for  $M \sim 10^4 M_\odot$ ) plus a nonthermal tail from jet-disk coupling (Makishima et al. 2000; Farrell et al. 2009).

Magnetars are typically isolated or in young supernova remnants/OB associations (Kaspi 2010). A bright optical/IR counterpart showing magnetospheric pulsations ( $\sim$ s) would favor a magnetar. In contrast, an IMBH in a dwarf galaxy or globular cluster may be optically faint ( $M_V > -2$ ) or undetected at 4.5

kpc (Mezcua 2017). Deep HST or 8 m-class imaging: detection of an OB companion or SNR shell implies a magnetar; absence of a stellar counterpart, possibly a faint extended cluster, favors the IMBH.

### Appendix B.2: White-Dwarf Model Versus IMBH Jet

Intermediate polar white dwarfs have  $P_{\text{spin}} \sim 10^2 - 10^3$  s and orbital periods  $P_{\text{orb}} \sim 10^4 - 10^5$  s. A beat between spin and orbital cannot naturally produce a strict 44 min ( $\sim 2640$  s) period without fine tuning (Patterson 1994; Qu & Zhang 2025). Such systems would also exhibit coherent pulsations at the white-dwarf spin ( $\sim 500$  s) or orbital ( $\sim 10^4$  s) periods in X-ray/optical light curves (Warner 1995). An IMBH jet model predicts none of these intermediate periods-only the 44 min precession and high-frequency flicker ( $< 10^2$  s). Searching for  $10^2 - 10^4$  s pulsations can thus discriminate a white-dwarf origin.

Achieving a stable  $\Delta t/P = 2/44$  min duty cycle over months would require an implausible long-term phase lock between spin and orbit in a white-dwarf system (Warner 1995), as tiny changes in  $\dot{P}$  or mass-transfer rate would break the 44 min clock. An LT-precessing IMBH disk is expected to maintain  $P_{\text{LT}}$  stably for  $10^4 - 10^6 t_g$  (Fragile et al. 2007; Liska et al. 2018). Monitoring the period over  $\gtrsim 6$  months: any  $\Delta P/P \gtrsim 1\%$  drift is inconsistent with LT precession but expected for white-dwarf spin evolution ( $\dot{P} \sim 10^{-11}$  s/s).

### Appendix B.3: Low-Mass XRB Versus IMBH

For a stellar-mass BH ( $m \sim 10$ ), Eq. (5) demands  $r \sim 443 R_g$  ( $R \sim 6.6 \times 10^3$  km) to satisfy  $P_{\text{LT}} = 44$  min. At such radii, the viscous timescale  $t_{\text{acc}}$  is  $\sim 11$  days (Fragile et al. 2007; Liska et al. 2019), preventing rigid precession. Known XRBs precess on much longer superorbital timescales (SS 433: 162 d; Her X-1: 35 d; LMC X-4: 30 d; SMC X-1: 60 d) (Margon 1984; Petterson 1975; Heemskerk & van Paradijs 1989; Clarkson et al. 2003). Thus  $10 - 30 M_\odot$  XRBs cannot explain a 44 min precession.

Moreover, a ten-solar-mass XRB jet at  $r \sim 443 R_g$  would have too low  $P_{\text{BZ}} (\sim 10^{31-33} \text{ erg/s})$  to power the observed  $L_X \sim 10^{34-36} \text{ erg/s}$  (Merloni et al. 2003). In canonical XRB behavior, a transition from the hard state (jet "on") to soft state (jet quenched) occurs over hours-days (Fender et al. 2004; Corbel et al. 2003), during which the radio flares vanish and the X-ray spectrum softens. Only if ASKAP J1832-0911 were to undergo such a state transition-suppressing the 2/44 pattern for days-weeks and later restoring it-could a low-mass XRB remain viable, a behavior not yet observed in this source.

In canonical XRB behavior, a transition from the low/hard state (jet active, hard X-ray power law) to the high/soft state (jet quenched, disk-dominated spectrum) occurs over hours-days (Fender et al. 2004; Corbel et al. 2003). During this transition, the flat-spectrum radio core disappears and the nonthermal X-ray tail softens (Belloni 2010). If ASKAP J1832-0911 were a ten-solar-mass XRB, the 2 min/44 min flares would persist until such a state transition, vanish for days-weeks, and only reappear after returning to the hard state over months-years (as seen in GRS 1915+105; Belloni et al. (2000)). No prolonged "off-period" has been observed to date. In the absence of any detected state transition, a  $10 - 30 M_\odot$  XRB interpretation is strongly disfavored. Only a future detection of jet quenching and spectral softening lasting days, followed by a re-establishment of the 2/44 pattern after years, could salvage the low-mass XRB scenario.